JCTC Journal of Chemical Theory and Computation

Article

pubs.acs.org/JCTC

Systematic Parameterization of Monovalent Ions Employing the Nonbonded Model

Pengfei Li, Lin Frank Song, and Kenneth M. Merz, Jr.*

Department of Chemistry and Department of Biochemistry and Molecular Biology, Michigan State University, East Lansing, Michigan 48824-1322, United States

Supporting Information

ABSTRACT: Monovalent ions play fundamental roles in many biological processes in organisms. Modeling these ions in molecular simulations continues to be a challenging problem. The 12−6 Lennard-Jones (LJ) nonbonded model is widely used to model monovalent ions in classical molecular dynamics simulations. A lot of parameterization efforts have been reported for these ions with a number of experimental end points. However, some reported parameter sets do not have a good balance between the two Lennard-Jones parameters (the van der Waals (VDW) radius and potential well depth), which affects their transferability. In the present work, via the use of a noble gas curve we fitted in former work (*J. Chem. Theory Comput.* **2013**, *9*, 2733), we reoptimized the 12−6 LJ parameters for 15 monovalent ions (11 positive and 4 negative ions) for three extensively used water models (TIP3P, SPC/E, and TIP4P$_{EW}$). Since the 12−6 LJ nonbonded model performs poorly in some instances for these ions, we have also parameterized the 12−6−4 LJ-type nonbonded model (*J. Chem. Theory Comput.* **2014**, *10*, 289) using the same three water models. The three derived parameter sets focused on reproducing the hydration free energies (the HFE set) and the ion−oxygen distance (the IOD set) using the 12−6 LJ nonbonded model and the 12−6−4 LJ-type nonbonded model (the 12−6−4 set) overall give improved results. In particular, the final parameter sets showed better agreement with quantum mechanically calculated VDW radii and improved transferability to ion-pair solutions when compared to previous parameter sets.

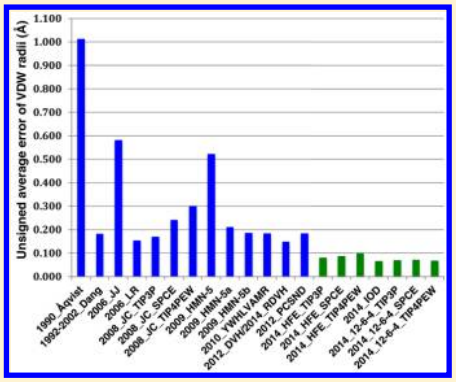

INTRODUCTION

Metal ions are extremely important in biological systems.[1−4] There are different ways to simulate these ions in biological systems using theoretical approaches. For example, quantum mechanical (QM) methods,[5,6] molecular mechanical (MM) methods,[7−9] and combined QM/MM methods.[10,11] For MM methods, there are a number of strategies that have been employed: the bonded model,[8,12−15] the nonbonded model,[9,16−20] the hybrid model,[21] the cationic dummy model,[7,22,23] the constrained nonbonded model,[24] the points-on-a-surface model,[25] and the polarizable model[26−28] all have been described and parameterized to study a broad range of metal containing complexes. The 12−6 Lennard-Jones (LJ) nonbonded model is widely used due to its simple form, ease to parameterize, speed advantage, and excellent transferability.[16−18,20] Monovalent ions such as Na^+, K^+, and Cl^- play significant roles and interact actively with nucleic acids, lipids, and proteins. Through the use of molecular dynamics (MD) simulations complex systems containing biological molecules and their associated counterions can be studied at the atomic level.[29−40] However, previously we found that the 12−6 LJ nonbonded model was unable to reproduce the experimental hydration free energy (HFE) and ion−oxygen distance (IOD) of the first solvation shell simultaneously for many ions due to an underestimation of the ion−water interaction energy.[9] This is mainly due to the fact that the 12−6 LJ potential does not include ion-induced dipole interactions, which should not be overlooked in highly polarized systems.[19] In light of this, we proposed a 12−6−4 LJ-type nonbonded model and parameterized it for divalent, trivalent, and tetravalent metal ions.[19,41] These parameters reproduced the experimental HFE and IOD values simultaneously.[19] Furthermore, tests in nucleic acid and protein systems further validated the new model.[19,41] In a further extension of our work, we have parameterized the 12−6 LJ and 12−6−4 LJ-type nonbonded models for 15 monovalent ions (11 positive ions and 4 negative ions) using similar methods as described previously.[9,19,41]

There are numerous systematic studies that have been reported in recent decades regarding the parameterization of the LJ nonbonded model for monovalent ions. For example, Åqvist pioneered the development of LJ parameters for the alkali and alkaline-earth metal cations.[16] Dang and co-workers developed a series of LJ parameters for alkali and halide ions from 1992 to 2012 for either nonpolarized or polarized water models.[42−49] Peng and Hagler parameterized the 9−6 potential for alkali metal cations and halide anions.[50] Jensen and Jorgensen have parameterized the LJ potential for the halide ions, alkali metal ions, and the ammonium ion using the TIP4P water model.[51] Roux and co-workers have parameterized the

Received: October 16, 2014
Published: February 6, 2015

DOI: 10.1021/ct500918t
J. Chem. Theory Comput. 2015, 11, 1645−1657

nonbonded model for the alkali and halide ions using the SWM4-DP polarized water model.[27,52] Joung and Cheatham have developed the LJ parameters for alkali cations and halide anions for three commonly used water models (TIP3P, SPC/E, and TIP4P$_{EW}$) for use in particle mesh Ewald (PME) simulation.[18] Netz and co-workers have designed different parameter sets for alkali ions in SPC/E water by treating single-ion and ion-pair properties as targets.[53] Hasse and co-workers have developed different parameter sets for the SPC/E water model in order to reproduce different experimental end points.[54,55] Reif and Hunenberger have created LJ nonbonded model parameters for alkali and halide ions using the SPC or SPC/E water model.[56] These parameters have been developed for different combining rules and simulation protocols. Various experimental/theoretical target values were used in the previous parameterization work to simulate ions in various environments (*e.g.*, the gas phase, liquid phase, and solid phase, interfacial phase, *etc.*). For example, quantum mechanically calculated gas-phase ion−water interaction energies for the monohydrates, experimental HFE, enthalpies and entropies, IOD and coordination number of the first solvation shell (CN), diffusion coefficients, mean residence times, radial distribution functions (RDFs), electric conductivity, dynamic hydration numbers, ion-pair properties, osmotic coefficients, lattice constants, and lattice energies, *etc.*.

Overall, it is hard to reproduce all of the available experimental/theoretical results at the same time due to accuracy limitations of the classical nonbonded model. Moreover, the reliability of the ion force field is water model specific making it better to design separate parameter sets for different water models due to their different parameter choices.[9,18,57] The present work concentrates on liquid simulations of the monovalent ions. We have parameterized three parameter sets (HFE, IOD, and the12−6−4 parameter sets) for 11 positive and 4 negative monovalent ions for three widely used water models (TIP3P, SPC/E, and TIP4P$_{EW}$), respectively. These parameters are specifically designed for the PME method,[58−60] which has become the standard approach to treat long-range electrostatics in MD simulations. Even so, there are innumerable combinations of the VDW radii and energy parameters ($R_{min}/2$ and ε) that can generate the same HFE or IOD values.[9,18] Hence, the balance of these two parameters is a significant consideration for their transferability to mixed systems.

In previous parameter sets, the parameters were usually designed using fixed ε values for all of the negative or positive ions.[49,51,54,55] Jensen and Jorgensen designed "big and small" ε parameters for negative and positive ions, respectively, in their parameterization work.[51] Joung and Cheatham have determined the parameters empirically based on a compromise between different experimental properties, including the HFE, IOD, lattice energies, and lattice constants.[18] For the alkali and halide ion series there is an apparent trend in this parameter set where as $R_{min}/2$ increases for the bigger ions, the ε parameter also increases.[18] In previous work, via a consideration of the physical meaning of the VDW interactions, we have fitted a curve to describe the relationship between the $R_{min}/2$ and ε values based on the experimental results for noble gas atoms.[9] By fitting a noble gas curve (NGC), we have determined the LJ parameters for the Lorentz−Berthelot (LB) combining rules for the various divalent, trivalent, and tetravalent metal ions.[9,41] The derived $R_{min}/2$ values coincide well with the VDW radii calculated using the quantum scaling principle (QMSP) method.[61] Herein, using the methods we employed previously,[9,19,41] we have designed parameters for 11 positive and 4 negative ions. Again, consistent results were obtained using this approach with the derived $R_{min}/2$ values corresponding to the VDW radii calculated by the QMSP method.[61] The unsigned average error (UAE) values of the present parameter sets are smaller than those based on other parameter sets with respect to the QMSP calculated VDW radii. We also carried out test simulations on six different ion solutions. Using the experimental activity derivative values as a basis for comparison, in general, our parameter sets showed better performance than the parameter sets of Joung and Cheatham[18] and Horinek et al.[53] This supports our assertion that the current parameters have better transferability due to a better balance between the $R_{min}/2$ and ε parameters. Meanwhile, the 12−6−4 parameter set showed the best performance among the investigated parameter sets, further illustrating it is a superior model relative to the 12−6 LJ nonbonded model.

METHODS

Potential Function and Combining Rules. In the present work we utilized the nonbonded model employed by the AMBER force field (eq 1).[62]

$$\begin{aligned} U_{ij}(r_{ij}) &= \frac{C_{12}^{ij}}{r_{ij}^{12}} - \frac{C_6^{ij}}{r_{ij}^{12}} - \frac{C_4^{ij}}{r_{ij}^{4}} + \frac{e^2 Q_i Q_j}{r_{ij}} \\ &= \varepsilon_{ij}\left[\left(\frac{R_{\min,ij}}{r_{ij}}\right)^{12} - 2\left(\frac{R_{\min.ij}}{r_{ij}}\right)^{6}\right] - \frac{C_4^{ij}}{r_{ij}^{4}} + \frac{e^2 Q_i Q_j}{r_{ij}} \\ &= 4\varepsilon_{ij}\left[\left(\frac{\sigma_{ij}}{r_{ij}}\right)^{12} - \left(\frac{\sigma_{ij}}{r_{ij}}\right)^{6}\right] - \frac{C_4^{ij}}{r_{ij}^{4}} + \frac{e^2 Q_i Q_j}{r_{ij}} \end{aligned} \quad (1)$$

In which r_{ij} is the distance between two particles i and j, and the Q_i and Q_j are the point charges of the two particles while e is the proton charge. For the metal ion, its point charge is usually treated as an integer number according to their oxidation state. The parameter $R_{min,ij}$ (or σ_{ij}) and ε_{ij} are the only two parameters that need to be determined. For $R_{min,ij}$ (or σ_{ij}), there are two combining rules; the Lorentz combining rule (see eq 2) and the Good−Hope combining rule (see eq 3) are widely used in MM simulations.

$$R_{\min,ij} = R_{\min,i} + R_{\min,j} \quad \text{or} \quad \sigma_{ij} = \sigma_i + \sigma_j \quad (2)$$

$$R_{\min,ij} = \sqrt{R_{\min,i} R_{\min,j}} \quad \text{or} \quad \sigma_{ij} = \sqrt{\sigma_i \sigma_j} \quad (3)$$

For the ε_{ij} (potential well depth) parameter, the Berthelot combining rule is commonly used (see eq 4).

$$\varepsilon_{ij} = \sqrt{\varepsilon_i \varepsilon_j} \quad (4)$$

The LB combining rules (eqs 2 and 4) is used in the AMBER[62] and CHARMM[63] force fields while the geometric-mean combining rule (eqs 3 and 4) is used in the OPLS-AA[64] force field. Parameters using one combining rule need to be modified when moving to the second combining rule. Herein all the simulations use the LB combining rules, but if one wants to use the geometric combining rules, they can adapt the parameters by using eqs 2−4.

Thermodynamics Integration. Thermodynamic integration[65−71] is a powerful tool to study the free energy difference of two different states of one system. It was used to simulate the

DOI: 10.1021/ct500918t
J. Chem. Theory Comput. 2015, 11, 1645−1657

hydration free energy in the present work. It employed a mixed potential for the initial and final states (V_0 and V_1, respectively, in eq 5). k is an integer number which equals 1 when linear mixing is employed, λ is a number between 0 and 1, representing the extent of mixing of the two states.

$$V(\lambda) = (1-\lambda)^k V_0 + [1-(1-\lambda)^k]V_1 \tag{5}$$

To simulate the particle disappearance or appearance process, the soft-core scaling method with linear mixing was utilized.[72] It employs a modified LJ potential which changes with the λ value (see eq 6). It prevents "end-point catastrophes" when we "turn on" the particle, thereby eliminating this artifact in an effective way.

$$V_{\text{soft-coreVDW}} = 4\varepsilon(1-\lambda)\left[\frac{1}{\left[\alpha\lambda + \left(\frac{r_{ij}}{\sigma}\right)^6\right]^2} - \frac{1}{\alpha\lambda + \left(\frac{r_{ij}}{\sigma}\right)^6}\right] \tag{6}$$

The free energy difference of two states is obtained by integration of $\partial V/\partial\lambda$ along the λ coordinate (eq 7). While in the present work we employed Gaussian quadrature to calculate the integration (eq 8, the w_i are the weights for the different i values).

$$\Delta A = A(\lambda{=}1) - A(\lambda{=}0) = \int_0^1 \langle \partial V/\partial\lambda\rangle_\lambda \, d\lambda \tag{7}$$

$$\Delta A = \sum w_i \langle \partial V/\partial\lambda\rangle_i \tag{8}$$

HFE Calculation. All simulations and analyses in the present work were carried out using the AMBER 12 and AmberTools 12 suite of programs.[62] For the HFE calculations, a dummy atom was solvated in a ~29 Å × 29 Å × 29 Å water box initially with the closest water 1.5 Å away from it. There are 721, 721, and 732 water molecules in the TIP3P, SPC/E, and $TIP4P_{EW}$ water boxes, respectively. Then 1000 steps of steepest descent minimization followed by 1000 steps of conjugate gradient minimization were performed to minimize the initial structure. Afterwards a 1 ns simulation in the *NVT* ensemble was carried out to gradually heat the system from 0 to 300 K followed by a 1 ns simulation in the *NPT* ensemble at 300 K and 1 atm to correct the density and to further equilibrate the system. The final snapshot was used as the initial structure for the *NPT* TI simulations. The HFE values were obtained according to the thermodynamic cycle shown in Figure 1. First a four-window linear soft-core set of simulations with λ values of 0.1127, 0.5, 0.88729, and 0.98 were performed to obtain the free energy change arising from "turning on" the VDW interaction between the dummy atom and surrounding particles. The final window was not considered in the free energy calculation but further equilibrated the system for the next stage of the free energy calculation. Afterward a nine-window linear TI calculation was performed with λ values of 0, 0.02544, 0.12923, 0.29707, 0.5, 0.70292, 0.87076. 0.97455, and 1 to obtain the ΔG_{ele} (or $\Delta G_{ele+pol}$ for the 12−6−4 nonbonded model). Then a reverse nine-window linear TI calculation was carried out to obtain the value of $-\Delta G_{ele}$ (or $-\Delta G_{ele+pol}$). Finally another three-window soft-core linear TI simulation with λ values of 0.1127, 0.5, and 0.88729 was performed to obtain the $-\Delta G_{VDW}$ value. For the VDW scaling part, each window was equilibrated for 100 ps followed by 200 ps of sampling while for the electrostatic scaling (or electrostatic plus polarization scaling) simulations, each window was equilibrated for 50 ps followed by 150 ps of sampling. In the end, the HFE values were evaluated based on the ΔG_{VDW}, ΔG_{ele} (or $\Delta G_{ele+pol}$), $-\Delta G_{ele}$ (or $-\Delta G_{ele+pol}$), and $-\Delta G_{VDW}$ values.

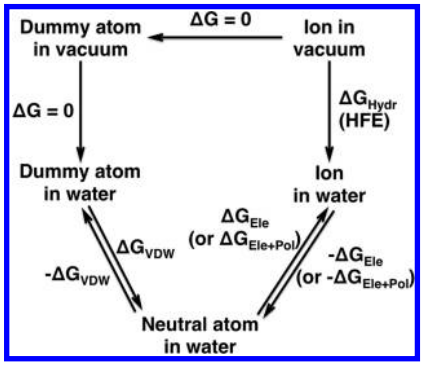

Figure 1. Thermodynamics cycle used to determined the HFE values.

There are two sets of uncertainty analyses we performed for the HFE simulations. Both analyses obtained the uncertainty of the VDW and electrostatic parts separately and yielded the total uncertainty by adding up the two contributions. The data sets for the two analyses are shown in two different spreadsheets in the Supporting Information (SI). The first method involves cutting the sampling into different pieces and then calculating the standard deviation between them. For the case where the VDW interaction is appearing, we treated the first 100 ps of sampling for each window as the first distribution, while the second 100 ps sampling as the second distribution. We then obtained the free energy of each part independently. For the situation where the VDW term is disappearing we used an identical protocol. Then the uncertainty of the VDW part of the TI calculations was obtained based on these four values (two where the VDW term "appears" and two where the VDW term "disappears"). The uncertainty for the electrostatic part of the TI calculations was obtained in a similar manner except we had 75 ps of sampling rather than 100 ps for each distribution.

$$\delta A = \sqrt{\langle A^2\rangle_c}\sqrt{\frac{2\tau_A}{T}} \tag{9}$$

The second method utilized eq 9 to evaluate the computational uncertainty. Herein the $\langle A^2\rangle_c$, τ_A, and T are the standard deviation, correlation time and sampling time of property A, respectively. δA is the computational uncertainty of A with the final data being represented as $\langle A\rangle \pm \delta A$. For the VDW step, τ_A was treated as 500 fs while for the electrostatic step (or electrostatic plus polarization step) it was treated as 250 fs. These values were obtained from test simulations and are consistent with the former research of Shirts et al.[73] The uncertainty values obtained for the first approach are in the range of 0.0−1.2 kcal/mol with an average value of 0.4 kcal/mol. The uncertainty values for the second approach are in the range of 0.5−0.8 kcal/mol with an average value of 0.6 kcal/mol. Based on these values we estimate that uncertainty of the calculated HFE values in the present work is ~1.0 kcal/mol.

IOD and CN Value Determination. A metal ion was solvated using the same water box size as indicated above. Then 2000 steps of minimization (1000 steps of steepest descent minimization followed by 1000 steps of conjugated gradient minimization) were performed. Afterward a 1 ns simulation in

DOI: 10.1021/ct500918t
J. Chem. Theory Comput. 2015, 11, 1645−1657

Table 1. Target Values of the HFE, IOD, and CN of the First Solvation Shell for Monovalent Ions

ions	mass (g/mol)	electronic structures	HFE(kcal/mol)[a]	IOD (Å)[b]	CN[b]
Li^+	6.94	[He]	−113.5	2.08 ± 0.06	4−6
Na^+	22.99	[Ne]	−87.2	2.35 ± 0.06	4−8
K^+	39.10	[Ar]	−70.5	2.79 ± 0.08	6−8
Rb^+	85.47	[Kr]	−65.7	2.89 ± 0.10	
Cs^+	132.91	[Xe]	−59.8	3.13 ± 0.07	7−8
Tl^+	204.38	[Xe] $4f^{14}5d^{10}6s^2$	−71.7	2.96[c]	4[c]
Cu^+	63.55	[Ar] $3d^{10}$	−125.5	1.87[d]	2[d]
Ag^+	107.87	[Kr] $4d^{10}$	−102.8	2.41 ± 0.02	2−4
NH_4^+	18.04		−68.1	2.85[e]	4−11[h]
H^+ (Zundel cation)	1.007		−251.0	1.24[f]	2[f]
H^+ (Eigen cation)	1.007		−251.0	1.01[g]	1[g]
H_3O^+	19.02		−103.4	2.75 ± 0.01	4
F^-	19.00	[Ne]	−119.7	2.63 ± 0.02	4.1−6.8
Cl^-	35.45	[Ar]	−89.1	3.18 ± 0.06	6−8.5
Br^-	79.90	[Kr]	−82.7	3.37 ± 0.05	6
I^-	126.9	[Xe]	−74.3	3.64 ± 0.03	6−8.7

[a]The HFE values of positive ions come from Marcus[78] while the HFE values of halide ions are from Schmid et al.[79] [b]From Marcus[78] unless specified otherwise. [c]Weighted average value of four bonds (two at 2.73 Å and two at 3.18 Å) from Persson et al.[87] [d]From Burda et al.[90] [e]Obtained by addition of the ionic radius of NH_4^+ from Detellier and Laszlo[91] and the effective ionic radius of O^{2-} from Pauling.[92] [f]From quantum calculations done by Meraj and Chaudhari.[95] [g]From Sobolewski and Domcke at the MP2/6-31+G** level of theory.[96] [h]From Ohtaki and Radnai.[99]

the *NVT* ensemble was carried out to heat the system from 0 to 300 K followed by a 1 ns simulation in the *NPT* ensemble at 300 K and 1 atm to correct the density and further equilibrate the system. Finally a 2 ns sampling simulation was performed in the *NPT* ensemble at 300 K and 1 atm with snapshots being stored every 500 fs. In total 4000 snapshots were obtained for the final analysis. From these snapshots the RDF of the metal ion and water oxygen atoms was obtained in the range of 0.0−8.0 Å with a resolution of 0.01 Å based on the average volume of the trajectory. Then the points within ±0.1 Å of the first peak (for a total of 21 points) were used in a quadratic fit. Afterward, a second quadratic fit was carried out based on the points, which are within ±0.1 Å of the apex (out to two decimal places) of the first quadratic fit. The apex of the second fit was chosen as the IOD value out to two decimal places. All CN values were obtained by integrating the RDF from its origin to the first minimum.

For the previous simulations (both the TI and MD simulations), the PME[58−60] method with periodic boundary conditions (PBC) was used in the MD simulations. The Langevin algorithm was used to control the temperature with a collision frequency of 5 ps^{-1}. For the MD simulations performed in the *NPT* ensemble, Berendsen's barostat with isotropic position scaling was utilized for pressure control with the relaxation time set as 10 and 1 ps for the TI and standard (which was used to obtain the IOD and CN) simulations, respectively. The time step was set to 1 fs for all of the MD simulations except for the simulations performed for the proton−water system using the 12−6−4 LJ-type potential, for which a 0.5 fs time step was used. The SHAKE algorithm[74] was used to constrain the distance between hydrogen atoms and their attached heavy atoms with a tolerance of 1.0×10^{-5} Å while the "three-site" algorithm was used for the water molecules.[75]

Ion Solution Simulation. OpenMM[76,77] (in version 6.1) was used for the ion solution simulations. Thirteen Na^+ ion and 13 Cl^- ions were solvated in a water box with a size of ∼46 Å × 46 Å × 46 Å, in which there are 2414 SPC/E water molecules (giving a molarity of ∼0.3 M). First 2000 steps of minimization employing the L-BFGS algorithm was used to optimize the structure; then 1 ns of *NVT* heating was performed with the temperature increasing gradually from 0 to 300 K. Then another 1 ns of simulation was performed to equilibrate the system in the *NVT* ensemble. Afterward 2 ns of equilibration was carried out followed by 10 ns of sampling in the *NPT* ensemble. One snapshot was stored for each 0.5 ps, yielding 20000 snapshots for the final analysis. A 10 Å cutoff was used for the nonbonded interaction. In order to be consistent with the parameterization simulations, a direct truncation algorithm was used for the C_4 terms. The PME method and PBC were used for the simulations, and the Langevin algorithm with a 1.0 ps^{-1} friction coefficient was used for the temperature control. A Monte Carlo barostat was used for pressure control with the volume change attempt frequency set at 25 fs^{-1}. The time step was 1.0 fs with SHAKE used to constrain the bonds containing hydrogen atoms.

The Kirkwood−Buff integrals were calculated based on eq 10; then the activity derivatives a_{cc} were obtained from eq 11.

$$G_{ij} = \int_0^\infty 4\pi r^2[g_{ij}(r) - 1]\,dr \tag{10}$$

$$a_{cc} = \frac{1}{1 + \rho_c(G_{cc} - G_{cw})} = \frac{1}{1 + N_{cc} - \frac{\rho_c N_{cw}}{\rho_w}} \tag{11}$$

$g_{ij}(r)$ is the radial distribution function between species i and j. dr was treated as 0.01 Å for the radial distribution function calculation, and the cutoff of the radial distribution was set to 12 Å. ρ_c and ρ_w are the number densities of the ion (here the positive and negative ions are treated as indistinguishable) and water, respectively, while N_{cc} and N_{cw} are the excess coordination numbers between the ion−ion and ion−water pairs.

RESULTS AND DISCUSSION

Targeted Values. There are different sets of experimental HFE values that exist in the literature for the monovalent ions.[78,79] Most of these values were obtained based on the proton's HFE value, but final agreement on this value has not

DOI: 10.1021/ct500918t
J. Chem. Theory Comput. 2015, 11, 1645−1657

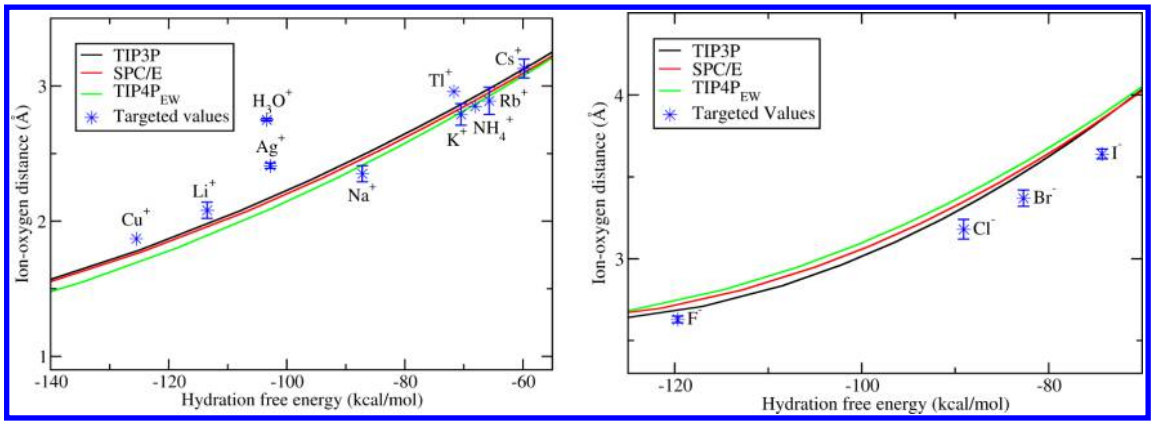

Figure 2. Fitting curves between the HFE and IOD values for the positive (left) and negative (right) monovalent ions with three water models together with the targeted values of the ions investigated in the present work.

been reached. The accepted range is between −250 to −265 kcal/mol.[56,78,80−83] In Reif and Hünenberger's work on the design of monovalent ion parameters,[56] they supported a value of −1100 kJ/mol (∼−263 kcal/mol). While in Lamoureux and Roux's work,[52] they used a value of −247 kcal/mol (∼−1033 kJ/mol) to develop a model which reproduced both gas- and aqueous-phase properties. Herein we use the experimental values from the work of Marcus[78] and Schmid et al.[79] (Table 1). For Marcus's HFE values,[78] the HFE of monovalent ions were obtained based on $\Delta_{hyd}G°(H^+)$ = −1056 kJ/mol (∼−252 kcal/mol) from $\Delta_{hyd}H°(H^+)$ = −1094 kJ/mol and $\Delta_{hyd}S°(H^+)$ = −131 J/(K·mol) or $S_\infty[H^+(aq)]$ = −22.2 J/(K·mol), while Schmid et al. refitted the HFE values of the atomic ions based on $\Delta_{hyd}H°(H^+)$ = −1078 kJ/mol.[79] For positive ions, there is a trivial difference (∼0.7 kcal/mol on average) between the data sets of Marcus and Schmid et al. We have used Marcus' HFE values as target values since this set is more complete. The HFE value of the H_3O^+ ion is from Palascak and Shields[84] due to its absence in the data sets of Marcus[78] and Schmid et al.[79] For the halide ions, Schmid et al.'s values are ∼8 kcal/mol lower than Marcus' values on average. Herein, we used Schmid et al.'s data set as our target since it is consistent with a broader range of experimental values.[18,85]

Most of the IOD values come from Marcus' review[86] except those of the Tl^+, Cu^+, NH_4^+, and H^+ ions. The Tl^+ ion is similar to the Sn^{2+} ion which all have a lone-pair electron in the outmost electron shell, resulting in the observation of two IODs in the first solvation shell in the aqueous phase. This effect is hard to reproduce using classical MD simulations due to the assumption of isotropic behavior. Typically, the reported CN value of the Tl^+ ion is between 6 and 8 while Persson et al. determined the CN of Tl^+ as 4 for aqueous systems.[87] In their work they found a four-coordinated Tl^+ ion with two different IOD values representing two water molecules at 2.73 Å and two at 3.18 Å. The IOD value of Tl^+ (2.96 Å) used in the present work is the average of these two values. Shannon calculated the effective ionic radii of six- and eight-coordinated Tl^+ ion as 1.50 and 1.59 Å, respectively.[88] By adding the effective ionic radius of O^{2-} (1.40 Å) from Pauling, we can estimate that the IOD values for Tl^+ are 2.90 and 2.99 Å for six- and eight-coordiante structures, respectively, which is consistent with the IOD value we are using (2.96 Å). Vchirawongkwin et al. performed QM/MM MD simulations on the aqueous Tl^+ system and observed two different IODs (with 2.79 and 3.16 Å) and determined the average CN as 5.9.[89] Their theoretical work supports the "structure-breaking" character for Tl^+ in the bulk system.[89] It is hard to obtain an IOD value for the Cu^+ ion since it is easily oxidized by water. The IOD value for Cu^+ used in the present work comes from quantum calculations of Burda et al.[90] There is no reliable experimental IOD value for NH_4^+. We estimated the IOD value (2.85 Å) based on the ionic radius of the NH_4^+ ion (1.45 Å) from Detellier and Laszlo[91] and the ionic radius of O^{2-} (1.40 Å) from Pauling.[92] This value is consistent with classical and Car−Parrinello MD (CPMD) simulations.[93,94] H^+ in aqueous solution is thought to exist either as the Zundel ($H_5O_2^+$), Eigen ($H_9O_4^+$) or hydronium ion (H_3O^+). The IOD value of H^+ in the Zundel form was obtained from the quantum calculations of Meraj and Chaudhari,[95] while the IOD value of H^+ in the Eigen ion was taken from the calculations of Sobolewski and Domcke done at the MP2/6-31+G** level of theory.[96] Blauth et al. investigated aqueous Ag^+ by using the quantum mechanical charge field (QMCF) MD method simulation, in which they found the CN of the first solvation shell to be 6. The Ag^+ ion also acts as a structure-breaking factor in the bulk system.[97] Blumberger et al. investigated the Cu^+, Cu^{2+}, Ag^+, and Ag^{2+} ions in the bulk systems using the CPMD simulation method, in which they found the CN of these ions to be 2, 5−6, 4, and 5, respectively.[98]

Parameter Space Scanning. In Joung and Cheatham's work, they found that different combinations of parameter pairs could reproduce the HFE values in the parameter space available.[18] We have also observed this effect in our work on divalent metal ions.[9] In light of this we need a way to constrain one of the parameters in a physically reasonable manner and then vary the remaining parameter. To accomplish this, we used the NGC, which we fitted using experimental LJ parameters of noble gas atoms,[9] to select an appropriate ε value followed by a one-dimensional scan over a series of $R_{min}/2$ values.

For the positive ions, we scanned the parameter space along two parallel curves using the Na^+ ion as our reference (mass of 22.99 g/mol). One curve was based on the 12−6 LJ potential while the other had a fixed C_4 term equal to 100 kcal/(mol·Å^4). We then scanned $R_{min}/2$ from 0.8 to 2.3 Å with a step size of 0.1 Å for both curves. Via linear interpolations from the 12−6 to the 12−6−4 curves we were able to obtain initial guesses for the final 12−6−4 parameter sets. We only carried out one scan at one mass since the atomic mass has only a small effect on the computed thermodynamic and structural properties. And for the negative ions, we also scanned along two parallel curves

DOI: 10.1021/ct500918t
J. Chem. Theory Comput. 2015, 11, 1645−1657

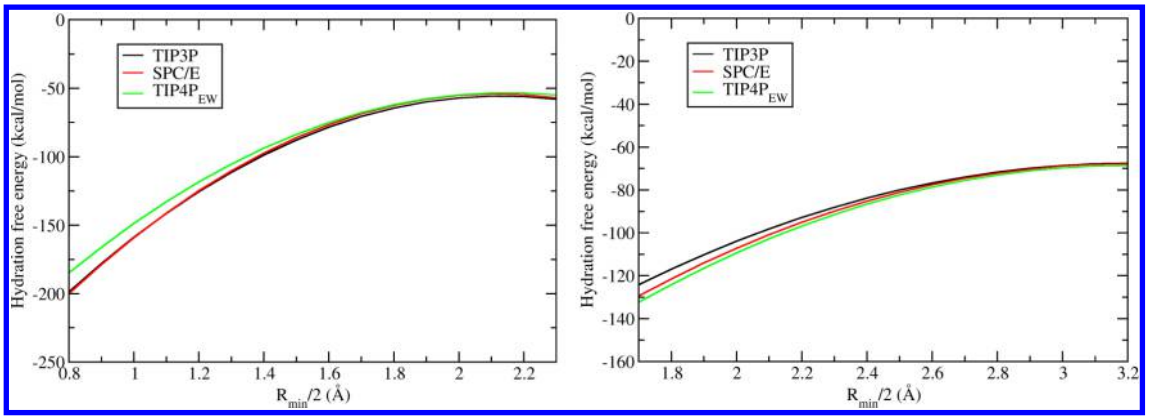

Figure 3. Fitting curves between the HFE and $R_{min}/2$ values for the positive (left) and negative (right) monovalent ions for three water models.

Table 2. Final Optimized HFE Parameter Set for Three Water Models

	TIP3P		SPC/E		TIP4P$_{EW}$	
	$R_{min}/2$ (Å)	ε (kcal/mol)	$R_{min}/2$ (Å)	ε (kcal/mol)	$R_{min}/2$ (Å)	ε (kcal/mol)
Li^+	1.267	0.00312065	1.258	0.00274091	1.226	0.00168686
Na^+	1.475	0.03171494	1.454	0.02639002	1.432	0.02154025
K^+	1.719	0.15131351	1.683	0.12693448	1.669	0.11803919
Rb^+	1.834	0.24140216	1.792	0.20665151	1.767	0.18689752
Cs^+	1.988	0.37853483	1.953	0.34673208	1.936	0.33132862
Tl^+	1.703	0.14021803	1.668	0.11741683	1.646	0.10417397
Cu^+	1.201	0.00112300	1.192	0.00096394	1.156	0.00050520
Ag^+	1.341	0.00818431	1.330	0.00716930	1.294	0.00452863
NH_4^+	1.779	0.19628399	1.743	0.16869420	1.707	0.14295367
H_3O^+	1.337	0.00780282	1.327	0.00691068	1.292	0.00440914
F^-	1.783	0.19945255	1.819	0.22878796	1.842	0.24821230
Cl^-	2.252	0.60293097	2.308	0.64367011	2.321	0.65269755
Br^-	2.428	0.72070940	2.470	0.74435812	2.520	0.77034233
I^-	2.724	0.85418187	2.770	0.86877007	2.819	0.88281946

using the Cl^- ion as our reference (mass of 35.45 g/mol). The first curve was also based on the 12−6 LJ potential while the second curve used a constant C_4 term of −100 kcal/(mol·Å^4). The range of $R_{min}/2$ is from 1.7 to 3.2 Å with a bin size of 0.1 Å. A larger $R_{min}/2$ range was chosen for the negative ions because, in general, they have a more dispersed electronic cloud. The parameters, and the simulated HFE, IOD, and CN values obtained from these parameter scans are shown in Tables SI.1 and SI.2 in the (SI).

Performance of the 12−6 LJ Nonbonded Model for the Monovalent Ions. First, we performed curve fits for HFE vs IOD along the scanning range for $R_{min}/2$ for both the positive and negative ions (see Figure 2). The experimental values are also shown in the figure (blue stars with error bars). There are different phenomena that have been observed for the positive and negative ions. For the positive ions, unlike the divalent or more highly charged ions,[9,41] the nonbonded model error is relatively small. For example, from Figure 2, we can see that it is possible to reproduce the targeted HFE and IOD values of Na^+, K^+, Rb^+, Cs^+, and NH_4^+ ions at the same time. Ramaniah et al. analyzed aqueous K^+ ion using *ab initio* MD and also demonstrated that classical potentials can yield good predictions for this ion,[100] while, for the Li^+, Tl^+, Cu^+, Ag^+, and H_3O^+ ions, the error is relatively large because of their stronger charge-induced dipole interactions with the surrounding water molecules. The proton is not shown in the figure because it is out of range. From later discussion, we note a 60−90 kcal/mol difference between the HFE value of the IOD parameter set and the experimental HFE value for the proton. Since, for almost half of the positive ions, it is possible to reproduce the IOD values using the HFE parameter set, we did not design a compromise parameter set due to the relatively small error of the 12−6 LJ nonbonded model for the monovalent ions. For the negative ions, the TIP3P water model showed the most consistency with the experimental values when employing the 12−6 LJ nonbonded model. It is intriguing that the 12−6 nonbonded model overestimated the HFE of the halide ions. It is hard to reproduce both the experimental HFE and IOD values simultaneously, and this may be due to the charge hydration asymmetry (CHA) effect, which is discussed further below.

Parameter Sets Developed in the Present Work. The parameter sets developed herein attempt to reproduce certain target values through a trial and error process. Based on the results of our parameter scans with the 12−6 LJ potential, we have fit curves of HFE vs $R_{min}/2$ for the positive and negative ions for three water models (see Figure 3). For the HFE fitting curves of the positive ions, the TIP3P and SPC/E water models are very close with each other with TIP4P$_{EW}$ being a little further away. This is consistent with our previous work.[9] Intriguingly, for the negative ions, the SPC/E and TIP4P$_{EW}$ water models are similar while the TIP3P water model gives more positive HFE values for the ions with the same LJ parameters. This may also come from the CHA effect (discussed later). Since there is a nontrivial difference between the three water models, we performed independent parameter-

DOI: 10.1021/ct500918t
J. Chem. Theory Comput. 2015, 11, 1645−1657

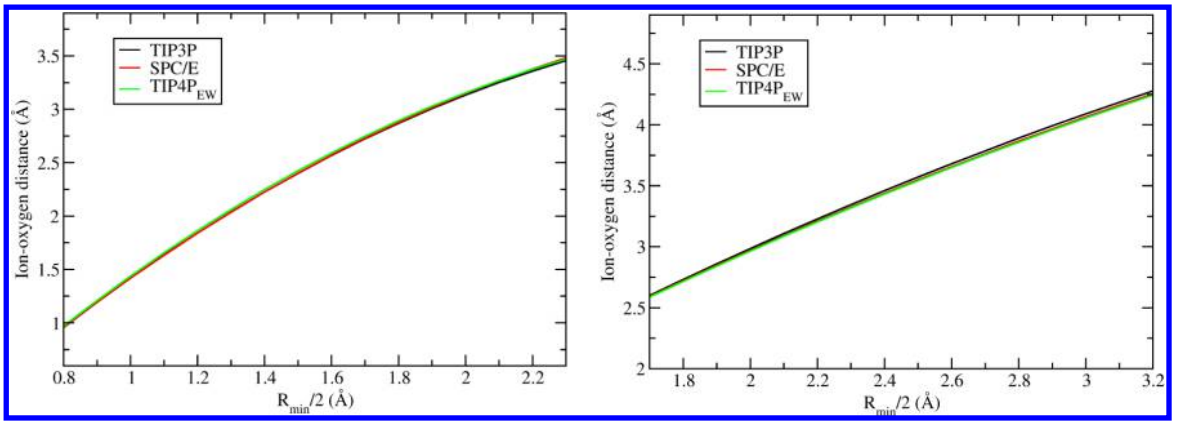

Figure 4. Fitting curves between the IOD and $R_{min}/2$ values for the positive (left) and negative (right) monovalent ions for three water models.

izations for these three water models separately to reproduce the experimental HFE values. The HFE parameter sets are shown in Table 2. Their corresponding simulated HFE, IOD, and CN values are given in SI Table SI.3a. These parameters reproduce HFE values within ±1.0 kcal/mol of the targeted values.

We also analyzed the IOD values vs $R_{min}/2$ values for the positive and negative ions for the three water models (see Figure 4). The three water models nearly share the same curve in the figure, for both the positive and negative ions. This is also consistent with our previous work on divalent metal ions.[9] The only difference between the positive and negative ions is that TIP4P$_{EW}$ predicts slightly larger IOD values for the positive ions and slightly smaller IOD values for the negative ions using the same LJ parameters that TIP3P and SPC/E do. Therefore, we designed a united IOD parameter set for all three water models. This parameter set is shown in Table 3 while the simulated HFE, IOD, and CN values are shown in SI Table SI.3b. The final IOD parameters reproduced the targeted IOD values within ±0.01 Å for most of the investigated ions in all of the water models.

Table 3. Final Optimized IOD Parameter Set Used for All Three Water Models

ions	$R_{min}/2$ (Å)	ε (kcal/mol)
Li^+	1.315	0.00594975
Na^+	1.465	0.02909167
K^+	1.745	0.17018074
Rb^+	1.820	0.22962229
Cs^+	2.000	0.38943250
Tl^+	1.870	0.27244486
Cu^+	1.214	0.00139196
Ag^+	1.500	0.03899838
NH_4^+	1.790	0.20504355
H^+ (Zundel cation)	0.925	0.00000147
H^+ (Eigen cation)	0.841	0.0000000661
H_3O^+	1.720	0.15202035
F^-	1.739	0.16573832
Cl^-	2.162	0.53154665
Br^-	2.331	0.65952968
I^-	2.590	0.80293907

The 12−6 LJ nonbonded model still shows some unsatisfactory behavior in that it underestimates (for some positive ions) or overestimates (for the negative ions) ion−water interactions, which lead us to build a 12−6−4 LJ-type nonbonded model for the monovalent ions investigated. The final parameters are shown in Table 4, while the corresponding computed HFE, IOD, and CN values are shown in SI Table SI.3c. These parameters simultaneously reproduce both targeted properties with considerable accuracy (within ±1.0 kcal/mol of the targeted HFEs and within ±0.01 Å of the targeted IODs). However, the situations are different for the positive and negative ions with respect to the obtained parameters. For the positive ions, the C_4 terms are always positive, while the C_4 terms are negative values for the negative ions. This arises from the fact that 12−6 LJ nonbonded model ignores the charge-induced dipole interaction for the positive ions, but overestimates the transfer effect for the negative ions (see later discussion). It is interesting that the C_4 term decreases as the ionic radii increases for the halide ions when using the TIP3P water model. While for the SPC/E and TIP4P$_{EW}$ water models the corresponding C_4 terms are very similar for different halide ions. In general, our parameter sets reproduce the targeted CN values with reasonable accuracy. The largest errors are found for the Tl^+, Cu^+, Ag^+, NH_4^+, and H_3O^+ ions, which are ions that do not share electronic structures with the noble gas atoms. The electronic structure of the outermost shell of Tl^+, Cu^+, and Ag^+ are $6s^2$, $3d^{10}$, and $4d^{10}$, respectively, while, for the NH_4^+ and H_3O^+ ions, it is hard to reproduce the hydrogen bond network because the current model does not reparameterize the hydrogen atoms explicitly. For the Tl^+ ion, the two different bond length values found in the first solvation shell of the Tl^+ ion were not reproduced in the present parameter sets due to the isotropic nature of the nonbonded model. For the Cu^+ ion, we could not reproduce the targeted CN value (which is 2) with any of the solvent models. In all cases the CN of the Cu^+ ion is 4. A similar situation has found for the Ag^+ ion where the experimental CN value ranges from 2 to 4 while our parameter sets give CNs from 4.8 to 6.0. Blauth et al. predicted the CN value of Ag^+ as 6.0 using QMCF MD simulations[97] while Blumberger et al. simulated the CN value of the Ag^+ ion as 4 in an aqueous system using the CPMD method.[98] It is hard to obtain the experimental CN values for the hydronium ion, but it has been proposed that the CN of water and the hydronium ion are similar to each other.[86] The HFE, IOD, and 12−6−4 parameter sets predict the CN values of the H_3O^+ ion in the ranges of 4.7−5.2, 7.0−7.1, and 8.2−8.4, respectively. The former one is consistent with the experimental CN values of water (determined as 5.2 from Soper[101]) while the later two CN values appear somewhat overestimated. The CN value of NH_4^+

DOI: 10.1021/ct500918t
J. Chem. Theory Comput. 2015, 11, 1645−1657

Table 4. Final Optimized 12-6-4 Parameter Set for the Three Water Models

	TIP3P			SPC/E			TIP4P$_{EW}$		
	$R_{min}/2$ (Å)	ε (kcal/mol)	C_4 (kcal/mol·Å^4)	$R_{min}/2$ (Å)	ε (kcal/mol)	C_4 (kcal/mol·Å^4)	$R_{min}/2$ (Å)	ε (kcal/mol)	C_4 (kcal/mol·Å^4)
Li^+	1.325	0.00674244	27	1.327	0.00691068	33	1.313	0.00580060	36
Na^+	1.473	0.03117732	0	1.472	0.03091095	6	1.459	0.02759452	9
K^+	1.758	0.17997960	8	1.760	0.18150763	19	1.751	0.17467422	24
Rb^+	1.831	0.23886274	0	1.826	0.23464849	7	1.817	0.22712223	13
Cs^+	2.008	0.39668797	2	2.004	0.39306142	12	1.997	0.38670945	16
Tl^+	1.893	0.29273756	50	1.889	0.28918714	61	1.883	0.28387745	65
Cu^+	1.217	0.00146124	7	1.218	0.00148497	9	1.214	0.00139196	21
Ag^+	1.533	0.05027793	83	1.536	0.05140063	92	1.522	0.04630154	94
NH_4^+	1.802	0.21475916	4	1.797	0.21069138	13	1.791	0.20584696	20
H^+ (Zundel cation)	0.992	0.00001138	108	0.987	0.00000988	106	0.997	0.00001309	126
H^+ (Eigen cation)	0.871	0.00000022	51	0.870	0.00000021	51	0.876	0.00000026	64
H_3O^+	1.774	0.19235093	190	1.773	0.19156806	205	1.770	0.18922704	209
F^-	1.725	0.15557763	−27	1.726	0.15629366	−53	1.728	0.15773029	−67
Cl^-	2.150	0.52153239	−38	2.153	0.52404590	−55	2.154	0.52488228	−66
Br^-	2.314	0.64785703	−39	2.324	0.65475744	−51	2.326	0.65612582	−68
I^-	2.567	0.79269938	−45	2.579	0.79809803	−51	2.585	0.80075128	−62

ion is in the range of 4−11 from the review of Ohtaki and Radnai,[99] and a CN value around 4−5 seems more reasonable due to hydrogen bond network considerations. Our parameter sets predict a CN in the range of 6.8−7.9 while CPMD simulations done by Brugé et al. predict a CN of 5.3.[94]

Percentage Errors of the Parameter Sets. To further assess the final parameter sets, we performed an error analysis. The resultant values are shown in SI Table SI.4. Using the TIP3P water model as an example, we depict the results of the error analysis in Figures 5 and 6. For the positive ions, the 12−6 LJ nonbonded model largely reproduces both the experimental HFE and IOD values for Na^+, K^+, Rb^+, Cs^+, and NH_4^+ ions while, for the Li^+, Tl^+, Ag^+, proton, and hydronium ions, the 12−6 LJ nonbonded model yields larger errors. Combining our present error analysis with previous ones,[9,41] we have summarized the estimated errors for the HFE and IOD parameter sets for the mono-, di-, tri-, and tetravalent positive ions in SI Table SI.5. Again using the TIP3P water model as an example, we graphically summarize our results in Figures 7 and 8. From these figures and SI Table SI.5 we observe, not surprisingly, that the average error values of the monovalent ions are significantly smaller than that of metal ions with higher oxidation states. The TIP3P and SPC/E water models show very similar results while the TIP4P$_{EW}$ water model shows the biggest deviation. From SI Table SI.5 and Figure 8 we observe that the extent of the underestimation of the absolute HFE values obtained using the IOD parameter sets increases roughly proportional to the square of the charge of the ions, which is consistent with the equation for the charge-induced dipole potential (eq 12). In eq 12, q is the charge of the charged ion while α_0 is the polarizability of the particle interacting with the ion. ε_0 and ε_r are the absolute vacuum permittivity and the relative permittivity, respectively. θ is the angle between the electric field generated by the ion and the induced dipole of the particle. For example, the ratio of the HFE underestimation obtained from the IOD parameter sets using the TIP3P water model is roughly 1.0:3.0:4.8:14.2 for monovalent to tetravalent ions (calculated from 17.2:51.1:82.7:244.3 kcal/mol). This trend is close to the ratio $1^2:2^2:3^2:4^2$, which is predicted from eq 12. This further validates the physical meaning of the C_4 term we have added for the 12−6−4 LJ-type potential.

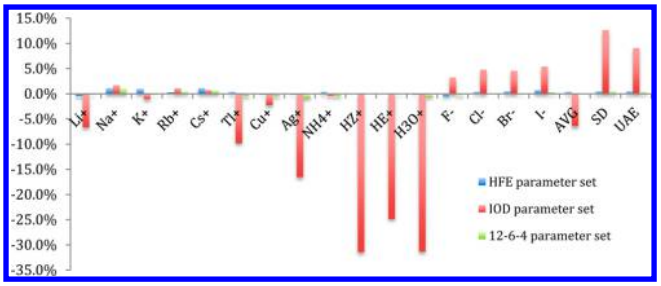

Figure 5. HFE percent error for different parameter sets for the monovalent ions with the TIP3P water model. HZ^+ and HE^+ represent the H^+ Zundel and Eigen ions, respectively. Since we did not design HFE parameter sets for the HZ^+ and HE^+ ions, they are not shown in the figure.

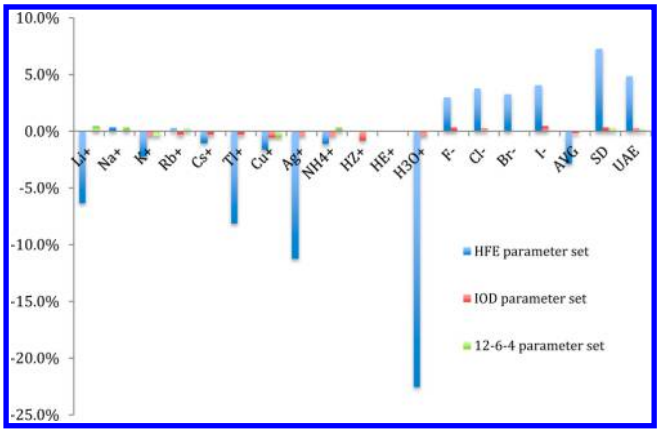

Figure 6. IOD percent error for different parameter sets for the monovalent ions with the TIP3P water model. HZ^+ and HE^+ represent the H^+ Zundel and Eigen ions, respectively. Since we did not design IOD parameter sets for the HZ^+ and HE^+ ions, they are not shown in the figure.

$$U_{q-\alpha_0} \approx -\frac{1}{2}\alpha_0\left(\frac{q}{4\pi\varepsilon_0\varepsilon_r r^2}\right)^2 \cos\theta \quad (12)$$

CHA Effect. Rajamani et al. explained that the CHA effect arises from two effects: (1) A positive electric potential is induced by surrounding water molecules on the surface of a

DOI: 10.1021/ct500918t
J. Chem. Theory Comput. 2015, 11, 1645−1657

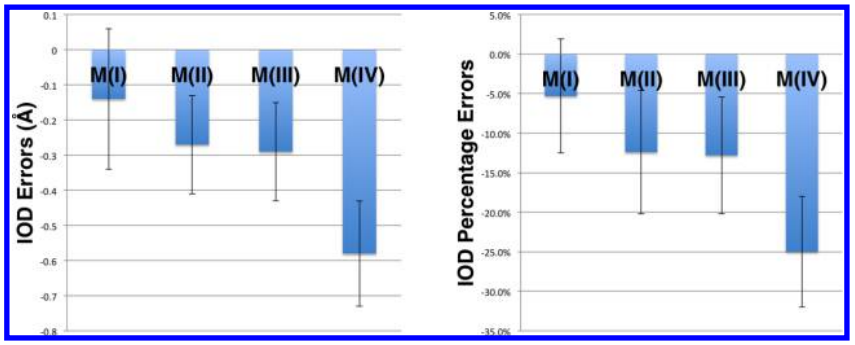

Figure 7. IOD absolute errors (left) and percentage errors (right) for the HFE parameter sets for the mono-, di-, tri-, and tetravalent cations in the TIP3P water model.

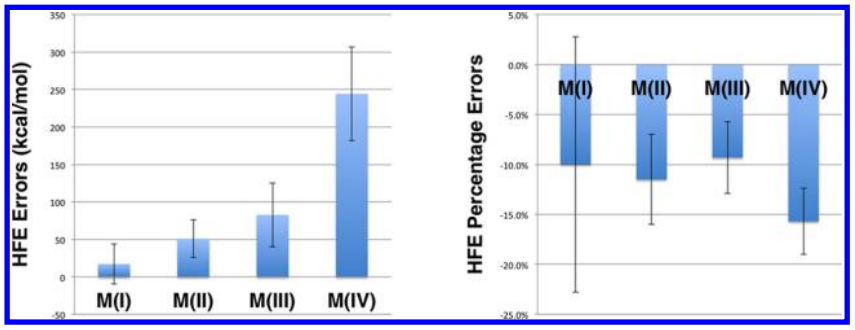

Figure 8. HFE absolute errors (left) and percentage errors (right) for the IOD parameter sets for the mono-, di-, tri-, and tetravalent cations in the TIP3P water model.

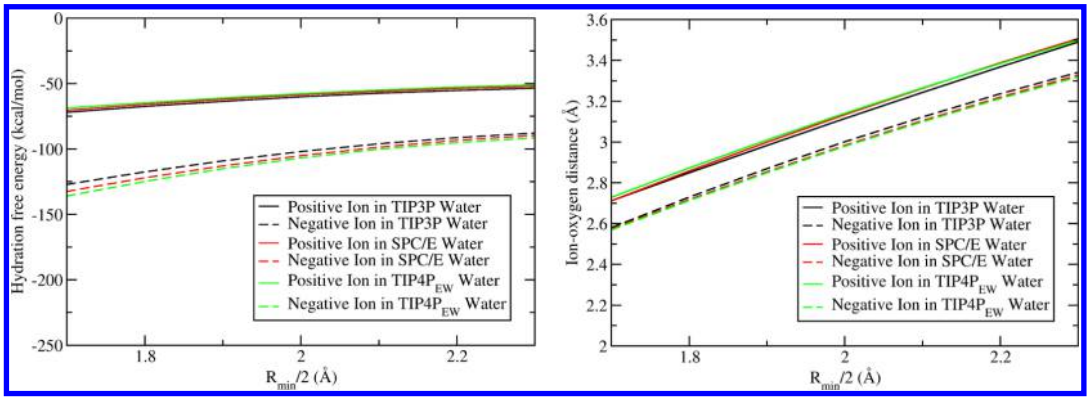

Figure 9. HFE vs $R_{min}/2$ fitting curve (left) and IOD vs $R_{min}/2$ fitting curve (right) for the positive and negative monovalent ions with different water models.

neutral solute, so more energy will be released when changing the neutral solute into a negatively charged one. (2) Water has different packing and orientations on the surface of positively and negatively charged solutes.[102] Onufriev and co-workers proposed that the CHA effect stems from the asymmetric electric multipole components of water molecules.[103] Later on their group developed a charge-asymmetric Born equation based on a statistical point of view, which incorporates the CHA effect efficiently. For aqueous systems containing ions, different atoms of the water molecule are coordinated to the counter ions due to their different electrical properties. For positive ions, it is the oxygen atoms, which have a partial negative charge, greater mass, and most of the electronic cloud coordinated to the counter ions. The opposite situation exists for the negative ions: it is the hydrogen atoms of the water molecules that orient toward the negative ions.

In the present work we employed explicit water models, which can model the CHA effect. Using the K^+ and F^- ions as examples, they have relatively similar effective radii[88] (1.38 and 1.33 Å), while the HFE difference between them is ∼41 or ∼49 kcal/mol based on Marcus' or Schmid et al.'s data sets. In the IOD parameter set, they almost have the same $R_{min}/2$ parameters (1.745 and 1.739 Å for K^+ and F^- ions respectively), while the computed HFE differences between them are ∼54, ∼61, and ∼65 kcal/mol for the TIP3P, SPC/E, and TIP4Pew water models, respectively. This is consistent with previous work that shows the TIP3P, SPC/E, and TIP4P water models have an increasing CHA effect.[102,103] From SI Table SI.3a we have collected the IOD values for the IOD parameter sets for the three water models. As we can see, unlike the positive ions, the IOD value sequence is TIP3P > SPC/E > $TIP4P_{EW}$ for the negative ions. This is opposite to the sequence of the hydrogen charge on these water models, which are 0.417

DOI: 10.1021/ct500918t
J. Chem. Theory Comput. 2015, 11, 1645−1657

e, 0.4238 *e*, and 0.52422 *e* for the TIP3P, SPC/E, and TIP4P$_{EW}$ water models, respectively. Hence, for the positive ions, it seems the dipole moment of the water molecules plays a dominant role for the solvation properties of the ions. On the other hand, for the negative ions, it appears that the charge of the hydrogen atoms is a dominant factor for the simulated properties of these ions.

To further clarify the CHA effect for the different water models employed herein, we have depicted the CHA effect using the data from our parameter scans and show the results in Figure 9. In this figure we observe that the CHA effect of the negative ions has smaller IOD and HFE values when compared to the positive ions employing the same LJ parameters. It is intriguing that this effect decreases considerably for the HFE values but not the IOD values as the ion's VDW radius increases.

The 12−6 LJ nonbonded model represents the interaction between an ion and its environment via a summation of the electronic and VDW terms. It does not consider polarization and charge-transfer effects explicitly, which may be the reason for the negative C_4 terms for the halide ions. For the cations, it is the oxygen atom that acts as the coordinated atom while it is the hydrogen atom coordinated to the counterion in the anion−water system. Since the electronic cloud focuses on the oxygen atoms, the charge-induced dipole cannot be overlooked for the positive ion−water systems. However, the polarization effect of the halide ion−water interaction should be relatively weak given the nature of the electron cloud on the hydrogen atoms in a water molecule.

Meanwhile, the charge-transfer effect behaves differently in ion−water systems for the positive and negative ions. The charge-transfer direction is from the water molecules to the ions for the former but in the opposite direction for the later systems. Thompson and Hynes found that, for anion−water systems, there is a charge transfer from the ion to the water, and this effect's strength decreases as the halide ion's size increases.[105] This is counterintuitive to what would be expected based solely on the electron affinity of the halogen atoms. They also found that when the distance between the halide ion and water is in the range of 0.7−1.0 Å, there is a strong polarization effect. However, as the distance continues to increase the charge-transfer effect becomes the dominant part where the charge is mainly transferred between the halide ion and the oxygen atom but not the hydrogen atoms of water.[105] Moreover, the closer the halide ion is to a water molecule, the stronger is the charge-transfer effect. The red shift caused by the charge-transfer effect is hard to simulate using only the 12−6 LJ nonbonded model while it is demonstrated that a mixed VB model is capable of reproducing the experimental red shift.[105] This is consistent with our observation that as the halide ion size increases, the trend of the HFE error of the IOD parameter set decreases (true for the SPC/E and TIP4P$_{EW}$ water models while it is almost a constant for the TIP3P water model). Taking the charge-transfer effect into account, the charge of the halide ions is less than $1e^-$ in aqueous solution, so the 12−6 LJ nonbonded model overestimates the halide ion−water interactions, making a negative C_4 term necessary in the 12−6−4 LJ-type nonbonded model.[106]

Consistency of the Parameter Sets. In parameter space, it is possible to reproduce the same properties using different combinations of the $R_{min}/2$ and ε values. This is because different $R_{min}/2$ and ε combinations can generate identical C_{12} values. Since the repulsion term plays a dominant role in the intermolecular distances, similar results can be obtained. However, a poor balance between the C_{12} and C_6 terms can cause transferability issues since all of the other C_{12} and C_6 values need to be calculated based on the combining rules for the mixed system. In this way, the balance of the C_{12} and C_6 terms plays a significant role in parameter transferability.

Our final parameter sets are consistent with each other since they were built in an analogous manner. In particular, they show a clear trend that when an ion has a bigger VDW radius, it generally has a deeper well depth. In the work of Peng et al., they proposed the following relationship between the VDW parameters of the ions which share the same electronic structure with specific noble gas atoms: (1) The ion radii and well depth should increase for the ions inside a group. (2) The ion radius of the negative ion should be bigger than the neutral atom and then the positive ion, which both have same electronic configuration. (3) The dispersion term should be bigger for the negative ion than for the neutral atom and the positive ion due to the extent of the electron cloud.[50] Our parameters follow these trends precisely.

Meanwhile, our parameters are also consistent with experimental results and theoretical calculations based on the QMSP method. For example, experimental results show that the F^- ion has smaller ionic radius than K^+ ion, and the IOD parameter set also shows this trend. The $R_{min}/2$ values of our parameter sets are more consistent with the VDW radii calculated by the QMSP method than the parameter sets presented elsewhere. The VDW radii calculated by Stokes based on the QMSP method[61] are shown in Table 5. In SI

Table 5. VDW Radii Calculated from the QMSP Method for the Ions Which Have the Same Electronic Structure with Noble Gas Atoms.[a]

ions	VDW radii (Å)[a]
Na^+	1.352
K^+	1.671
Rb^+	1.801
Cs^+	1.997
F^-	1.909
Cl^-	2.252
Br^-	2.298
I^-	2.548

[a]From Stokes.[61]

Table SI.6 we compare our parameters with the parameter sets developed by other groups (where we adapted their parameter sets for the LB combining rules). The average errors, standard deviation of the errors, and UAEs (using the QMSP VDW radii as reference values) of each parameter set were calculated and are given in SI Table SI.6. We show the unsigned average errors of the different parameter sets in Figure 10.

All of our parameter sets show the smallest UAE values (~0.08 Å) relative to earlier parameter sets. The metal ion parameters available in AMBER, which we adopted from the pioneering work of Åqvist where he fit the ions using a cutoff procedure (this was done prior to the emergence of the PME method), show the largest UAE. In this parameter set there is an imbalance between C_{12} and C_6, in which, the C_6 value is too small, while the C_{12} value is closer to our values (based on the relative ratio). Because of this the transferability of the parameter set will be affected since $R_{min,ij}$ is overestimated due to the too small C_6 value (recall $R_{min,ij} = (2C_{12,ij}/C_{6,ij})^{1/6}$).

DOI: 10.1021/ct500918t
J. Chem. Theory Comput. 2015, 11, 1645−1657

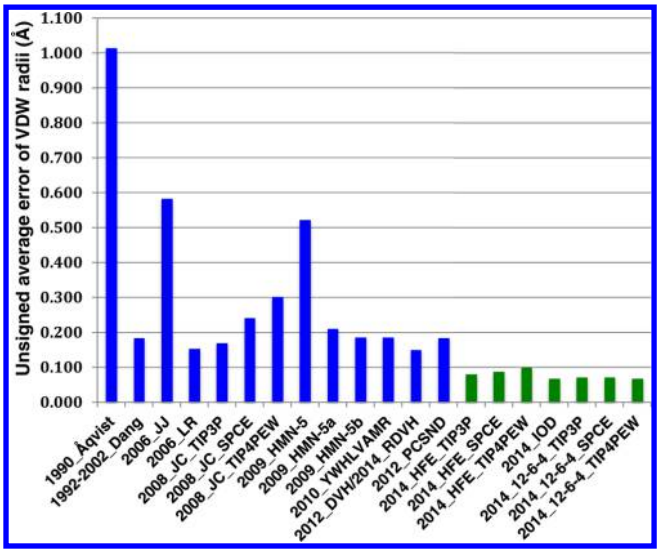

Figure 10. Unsigned average error of the VDW radii of different parameter sets using Table 5 as reference. The parameter sets developed herein are shown in the seven green columns on the right side of the figure.

For example, this causes the alkali ions to have an inverse trend among the ε parameters. The Jensen parameter set has a relatively large UAE due to the choice of the ε values for the positive ions (it is too small). The UAE of the VDW radii of the positive ions is ~1.08 Å while the corresponding UAE of the negative ions is only ~0.08 Å. This is because the ε value of the positive ions (which is 0.0005 kcal/mol) is too small while the ε value of the negative ions (which is 0.71 kcal/mol) is more reasonable. The large UAE value for the parameter set 5 of Netz and co-workers (2009_HMN-5) is due to the small ε value for the positive ions (~0.0006 kcal/mol).[53] The parameter sets from Joung and Cheatham also have too small ε values for the halide ions; for example, the ε value of Na^+ is always bigger than that of F^- (~30−100 times).[18] Dang's parameter sets also show small UAE values because its ε values are in the range of 0.1−0.2 kcal/mol,[42−49] which is reasonable for the monovalent ions.

Ion Solution Simulations. To further validate our parameter sets, we have carried out MD simulations of different ion-pair solutions. The Kirkwood−Buff (KB) integrals were calculated to investigate the ionic solution system. Finally the activity derivative was computed to evaluate the parameter sets. In the work of Moučka et al.,[107] they found the parameter set from Joung and Cheatham[18] (the JC parameter set herein) and the parameter set 5b from Horinek et al.[53] (the H2 parameter set herein; the values were adopted using LB combining rules and are shown in SI Table SI.8) are the best among 13 different parameter sets for simulating NaCl solutions with the SPC/E water model. In the work of Fyta and Netz, they reoptimized the mixing rules of the ion pairs to reproduce the activity derivative of several different kinds of ion solutions.[108] They found it was hard to reproduce the experimental activity derivatives of the NaF, KF, NaI, and CsI ion solutions. When compared to the values obtained using the unoptimized LB combining rules, they found that a larger ε_{ij} value for NaF, a larger $R_{\min,ij}$ value for KF, and a smaller ε_{ij} value for NaI and CsI were necessary to reproduce the experimental activity derivatives.

In the present work, we have carried out simulations on NaCl, KCl, NaF, KF, NaI, and CsI ion solutions at a concentration of ~0.30 M. The SPC/E water model was used in these simulations. The simulation details are detailed in Methods. Comparison between our parameter sets (HFE, IOD, and the 12−6−4 parameter sets for the SPC/E water model) with the JC and H2 parameter sets were made and are shown in Table 6. Herein we are using eq 13 (for the C_4 term for the ion

Table 6. Activity Derivatives for Six Different Ion Solutions in the SPC/E Water Model (Under ~0.3 M Condition)

	JC	H2	HFE	IOD	12-6-4	exptl values[a]
NaCl	1.08	1.00	1.00	1.03	1.01	0.93
KCl	1.11	1.13	1.03	1.07	0.91	0.90
NaBr	1.07	1.16	1.06	1.00	1.06	0.94
KF	0.87	0.76	0.84	0.87	0.86	0.92
NaI	0.93	0.98	0.87	0.90	0.93	0.97
CsI	0.87	1.09	1.03	0.97	0.92	0.86
av error	0.07	0.10	0.05	0.05	0.03	
SD	0.08	0.09	0.04	0.04	0.04	
UAE	0.10	0.15	0.11	0.09	0.06	

[a]From the book of Robinson and Stokes.[111]

with itself and the ion with the water hydrogen atoms) and eq 14 (for the C_4 term between the positive and negative ions) to estimate the C_4 terms between the particle pairs. The C_4 terms between the ions and oxygen atom in water are from Table 4. In the initial tests, we treated the tunfactor as 1.0 in eqs 12 and 13.

$$C_4(\text{atom type}) = \frac{C_4(H_2O)}{\alpha_0(H_2O)} \times \alpha_0(\text{atom type}) \times \text{tunfactor} \quad (13)$$

$$C_4 = \left(\frac{C_4^X(H_2O)}{\alpha_0(H_2O)} \alpha_0(M) + \frac{C_4^M(H_2O)}{\alpha_0(H_2O)} \alpha_0(X) \right) \times \text{tunfactor} \quad (14)$$

We set the polarizability of water to 1.444 $Å^3$, which was taken from Eisenberg and Kauzmann,[109] while the polarizability values of various monovalent ions were taken from Sangster and Atwood.[110] Since the electron cloud almost centers on the oxygen atoms in water, here we treated the oxygen atom as having all of the polarizability of the water molecule while the hydrogen atoms have a polarizability value equal to zero.

From Table 6 we can see that the average errors of the parameter sets follow the sequence 12−6−4 < HFE ~ IOD < JC < H2 while the UAEs follow the trend of 12−6−4 < IOD < JC < HFE < H2. In general our three parameter sets showed improved results over the JC and H2 parameter sets, indicating superior transferability. Indeed, the 12−6−4 parameter set showed the best performance among these parameter sets. Besides its better performance in simulating the single-ion properties, it also showed improved results in reproducing the ion-pair properties, further validating its advantage in simulating metal ions.

CONCLUSION

In the present work we have parameterized the 12−6 LJ and 12−6−4 LJ-type nonbonded models for 15 monovalent ions (11 cations with 4 anions) for three extensively used water models (TIP3P, SPC/E, and $TIP4P_{EW}$ water models).

DOI: 10.1021/ct500918t
J. Chem. Theory Comput. 2015, 11, 1645−1657

Compared to the highly charged ions, the 12−6 LJ nonbonded model gives rise to smaller errors for the monovalent ions. For some of the ions, it is possible to reproduce both the experimental HFE and IOD values simultaneously by employing the 12−6 LJ nonbonded model. In the end, three parameter sets (HFE, IOD, and 12−6−4 parameter sets) were developed for these ions. The HFE and IOD parameter sets are designed to reproduce the target HFE and IOD values, respectively, while the 12−6−4 parameter sets have been parameterized to reproduce both the experimental HFE and IOD values simultaneously.

The CHA phenomenon has been observed for the ions in the explicit water models we have investigated. Our results indicate that the CHA effect increases along the series TIP3P, SPC/E, and TIP4P$_{EW}$ with the TIP3P water model having the smallest error when compared to experimental results. We have compared our final parameter sets with previous sets from a number of research groups. Using the VDW radii calculated by the QMSP method as target values, we find that our parameter sets show the smallest UAE among all of the parameter sets investigated. This arises due to a better balance between the $R_{min}/2$ and ε values in our parameter sets. Furthermore, we predicted the activity derivatives for six different ion solutions and showed that the parameter sets developed herein (HFE, IOD, and 12−6−4) reproduced these quantities better than existing parameter sets, validating their improved transferability. The 12−6−4 parameter set showed the best performance over all of the parameter sets, further validating its advantage over the 12−6 LJ model. We believe that the parameter sets developed herein will improve our ability to model ions in biological systems.

■ ASSOCIATED CONTENT

Supporting Information

Tables listing computed HFE, IOD, and CN values of the parameter space scans each of the final determined parameter sets, errors for the parameter sets, VDW radii, water model parameters, H2 parameter set for the ions, and two sets of uncertainty values of each simulated HFE value. This material is available free of charge via the Internet at http://pubs.acs.org.

■ AUTHOR INFORMATION

Corresponding Author

*E-mail: kmerz1@gmail.com.

Funding

We appreciate the financial support from the National Health Institute (RO1's GM044974 and GM066859) and computational supports from the high performance computing centers at University of Florida and Michigan State University.

Notes

The authors declare no competing financial interest.

■ ACKNOWLEDGMENTS

We thank Dr. David Case (Rutgers) and Dr. Jason Swails (Rutgers) for help with modifying AMBER. We also thank Dr. Jason Swails for help with OpenMM. We thank Shuai Wang (UF) for help with writing some of the analysis code.

■ ABBREVIATIONS

LJ, Lennard-Jones; VDW, van der Waals; HFE, hydration free energy; IOD, ion−oxygen distance; RDF, radial distribution function; CN, coordination number; TI, thermodynamic integration; PME, particle mesh Ewald; CHA, charge hydration asymmetry; QMSP, quantum scaling principle

■ REFERENCES

(1) Thomson, A. J.; Gray, H. B. *Curr. Opin. Chem. Biol.* **1998**, *2*, 155−158.
(2) Rosenzweig, A. C. *Chem. Biol.* **2002**, *9*, 673−677.
(3) Waldron, K. J.; Robinson, N. J. *Nat. Rev. Microbiol.* **2009**, *7*, 25−35.
(4) Tus, A.; Rakipović, A.; Peretin, G.; Tomić, S.; Šikić, M. *Nucleic Acids Res.* **2012**, *40*, W352−W357.
(5) Dudev, T.; Lim, C. *Chem. Rev.* **2003**, *103*, 773−788.
(6) Dudev, T.; Lim, C. *Chem. Rev.* **2014**, *114*, 538−556.
(7) Pang, Y.-P. *Proteins: Struct., Funct., Bioinf.* **2001**, *45*, 183−189.
(8) Peters, M. B.; Yang, Y.; Wang, B.; Füsti-Molnár, L. S.; Weaver, M. N.; Merz, K. M., Jr. *J. Chem. Theory Comput.* **2010**, *6*, 2935−2947.
(9) Li, P.; Roberts, B. P.; Chakravorty, D. K.; Merz, K. M., Jr. *J. Chem. Theory Comput.* **2013**, *9*, 2733−2748.
(10) Wu, R.; Hu, P.; Wang, S.; Cao, Z.; Zhang, Y. *J. Chem. Theory Comput.* **2009**, *6*, 337−343.
(11) Hofer, T. S.; Weiss, A. K.; Randolf, B. R.; Rode, B. M. *Chem. Phys. Lett.* **2011**, *512*, 139−145.
(12) Hoops, S. C.; Anderson, K. W.; Merz, K. M., Jr. *J. Am. Chem. Soc.* **1991**, *113*, 8262−8270.
(13) Roberts, B. P.; Miller, B. R., III; Roitberg, A. E.; Merz, K. M., Jr. *J. Am. Chem. Soc.* **2012**, *134*, 9934−9937.
(14) Chakravorty, D.; Wang, B.; Lee, C.; Guerra, A.; Giedroc, D.; Merz, K., Jr. *J. Biomol. NMR* **2013**, 1−13.
(15) Ucisik, M. N.; Chakravorty, D. K.; Merz, K. M., Jr *Biochemistry* **2013**, *52*, 6911−6923.
(16) Åqvist, J. *J. Phys. Chem.* **1990**, *94*, 8021−8024.
(17) Stote, R. H.; Karplus, M. *Proteins: Struct., Funct., Bioinf.* **1995**, *23*, 12−31.
(18) Joung, I. S.; Cheatham, T. E. *J. Phys. Chem. B* **2008**, *112*, 9020−9041.
(19) Li, P.; Merz, K. M., Jr. *J. Chem. Theory Comput.* **2014**, *10*, 289−297.
(20) Merz, K. M., Jr. *J. Am. Chem. Soc.* **1991**, *113*, 406−411.
(21) Chakravorty, D. K.; Wang, B.; Ucisik, M. N.; Merz, K. M., Jr. *J. Am. Chem. Soc.* **2011**, *133*, 19330−19333.
(22) Saxena, A.; Sept, D. *J. Chem. Theory Comput.* **2013**, *9*, 3538−3542.
(23) Duarte, F.; Bauer, P.; Barrozo, A.; Amrein, B. A.; Purg, M.; Åqvist, J.; Kamerlin, S. C. L. *J. Phys. Chem. B* **2014**, *118*, 4351−4362.
(24) Hu, L.; Ryde, U. *J. Chem. Theory Comput.* **2011**, *7*, 2452−2463.
(25) Hay, B. P. *Coord. Chem. Rev.* **1993**, *126*, 177−236.
(26) Sakharov, D. V.; Lim, C. *J. Comput. Chem.* **2009**, *30*, 191−202.
(27) Yu, H.; Whitfield, T. W.; Harder, E.; Lamoureux, G.; Vorobyov, I.; Anisimov, V. M.; MacKerell, A. D.; Roux, B. t. *J. Chem. Theory Comput.* **2010**, *6*, 774−786.
(28) Zhang, J.; Yang, W.; Piquemal, J.-P.; Ren, P. *J. Chem. Theory Comput.* **2012**, *8*, 1314−1324.
(29) Allen, T. W.; Kuyucak, S.; Chung, S.-H. *Biophys. J.* **1999**, *77*, 2502−2516.
(30) Roux, B.; MacKinnon, R. *Science* **1999**, *285*, 100−102.
(31) Shrivastava, I. H.; Sansom, M. S. *Biophys. J.* **2000**, *78*, 557−570.
(32) Shrivastava, I. H.; Peter Tieleman, D.; Biggin, P. C.; Sansom, M. S. *Biophys. J.* **2002**, *83*, 633−645.
(33) Auffinger, P.; Bielecki, L.; Westhof, E. *J. Mol. Biol.* **2004**, *335*, 555−571.
(34) Cheatham, T. E., III *Curr. Opin. Struct. Biol.* **2004**, *14*, 360−367.
(35) Várnai, P.; Zakrzewska, K. *Nucleic Acids Res.* **2004**, *32*, 4269−4280.
(36) Gurtovenko, A. A. *J. Chem. Phys.* **2005**, *122*, No. 244902.
(37) Gurtovenko, A. A.; Miettinen, M.; Karttunen, M.; Vattulainen, I. *J. Phys. Chem. B* **2005**, *109*, 21126−21134.
(38) Vrbka, L.; Jungwirth, P.; Bauduin, P.; Touraud, D.; Kunz, W. *J. Phys. Chem. B* **2006**, *110*, 7036−7043.

DOI: 10.1021/ct500918t
J. Chem. Theory Comput. 2015, 11, 1645−1657

(39) Fowler, P. W.; Tai, K.; Sansom, M. S. *Biophys. J.* **2008**, *95*, 5062−5072.
(40) Egwolf, B.; Roux, B. *J. Mol. Biol.* **2010**, *401*, 831−842.
(41) Li, P.; Song, L. F.; Merz, K. M., Jr. *J. Phys. Chem. B* **2015**, *119*, 883−895.
(42) Dang, L. X. *J. Chem. Phys.* **1992**, *96*, 6970−6977.
(43) Dang, L. X.; Garrett, B. C. *J. Chem. Phys.* **1993**, *99*, 2972−2977.
(44) Dang, L. X. *Chem. Phys. Lett.* **1994**, *227*, 211−214.
(45) Smith, D. E.; Dang, L. X. *J. Chem. Phys.* **1994**, *100*, 3757−3766.
(46) Dang, L. X. *J. Am. Chem. Soc.* **1995**, *117*, 6954−6960.
(47) Chang, T.-M.; Dang, L. X. *J. Phys. Chem. B* **1999**, *103*, 4714−4720.
(48) Dang, L. X. *J. Phys. Chem. B* **2002**, *106*, 10388−10394.
(49) Peng, T.; Chang, T.-M.; Sun, X.; Nguyen, A. V.; Dang, L. X. *J. Mol. Liq.* **2012**, *173*, 47−54.
(50) Peng, Z.; Ewig, C. S.; Hwang, M.-J.; Waldman, M.; Hagler, A. T. *J. Phys. Chem. A* **1997**, *101*, 7243−7252.
(51) Jensen, K. P.; Jorgensen, W. L. *J. Chem. Theory Comput.* **2006**, *2*, 1499−1509.
(52) Lamoureux, G.; Roux, B. *J. Phys. Chem. B* **2006**, *110*, 3308−3322.
(53) Horinek, D.; Mamatkulov, S. I.; Netz, R. R. *J. Chem. Phys.* **2009**, *130*, 124507−124521.
(54) Deublein, S.; Vrabec, J.; Hasse, H. *J. Chem. Phys.* **2012**, *136*, 084501−084510.
(55) Reiser, S.; Deublein, S.; Vrabec, J.; Hasse, H. *J. Chem. Phys.* **2014**, *140*, No. 044504.
(56) Reif, M. M.; Hunenberger, P. H. *J. Chem. Phys.* **2011**, *134*, 144104−144125.
(57) Joung, I. S.; Cheatham, T. E., III. *J. Phys. Chem. B* **2009**, *113*, 13279−13290.
(58) Darden, T.; York, D.; Pedersen, L. *J. Chem. Phys.* **1993**, *98*, 10089−10092.
(59) Cheatham, T. E., III; Miller, J. L.; Fox, T.; Darden, T. A.; Kollman, P. A. *J. Am. Chem. Soc.* **1995**, *117*, 4193−4194.
(60) Petersen, H. G. *J. Chem. Phys.* **1995**, *103*, No. 3668.
(61) Stokes, R. *J. Am. Chem. Soc.* **1964**, *86*, 979−982.
(62) Case, D. A.; Cheatham, T. E.; Darden, T.; Gohlke, H.; Luo, R.; Merz, K. M.; Onufriev, A.; Simmerling, C.; Wang, B.; Woods, R. J. *J. Comput. Chem.* **2005**, *26*, 1668−1688.
(63) MacKerell, A. D.; Bashford, D.; Bellott, M.; Dunbrack, R.; Evanseck, J.; Field, M. J.; Fischer, S.; Gao, J.; Guo, H.; Ha, S. A. *J. Phys. Chem. B* **1998**, *102*, 3586−3616.
(64) Jorgensen, W. L.; Maxwell, D. S.; Tirado-Rives, J. *J. Am. Chem. Soc.* **1996**, *118*, 11225−11236.
(65) Mezei, M. *J. Chem. Phys.* **1987**, *86*, 7084−7088.
(66) Straatsma, T. P.; Berendsen, H. J. C. *J. Chem. Phys.* **1988**, *89*, 5876−5886.
(67) Mitchell, M. J.; McCammon, J. A. *J. Comput. Chem.* **1991**, *12*, 271−275.
(68) Kollman, P. *Chem. Rev.* **1993**, *93*, 2395−2417.
(69) Beutler, T. C.; Mark, A. E.; van Schaik, R. C.; Gerber, P. R.; van Gunsteren, W. F. *Chem. Phys. Lett.* **1994**, *222*, 529−539.
(70) Hummer, G.; Szabo, A. *J. Chem. Phys.* **1996**, *105*, 2004−2010.
(71) Simonson, T.; Carlsson, J.; Case, D. A. *J. Am. Chem. Soc.* **2004**, *126*, 4167−4180.
(72) Steinbrecher, T.; Mobley, D. L.; Case, D. A. *J. Chem. Phys.* **2007**, *127*, 214108−214113.
(73) Shirts, M. R.; Pitera, J. W.; Swope, W. C.; Pande, V. S. *J. Chem. Phys.* **2003**, *119*, 5740−5761.
(74) Ryckaert, J.-P.; Ciccotti, G.; Berendsen, H. J. *J. Comput. Phys.* **1977**, *23*, 327−341.
(75) Miyamoto, S.; Kollman, P. A. *J. Comput. Chem.* **1992**, *13*, 952−962.
(76) Eastman, P.; Pande, V. *Comput. Sci. Eng.* **2010**, *12*, 34−39.
(77) Eastman, P.; Friedrichs, M. S.; Chodera, J. D.; Radmer, R. J.; Bruns, C. M.; Ku, J. P.; Beauchamp, K. A.; Lane, T. J.; Wang, L.-P.; Shukla, D. *J. Chem. Theory Comput.* **2012**, *9*, 461−469.
(78) Marcus, Y. *J. Chem. Soc., Faraday Trans.* **1991**, *87*, 2995−2999.
(79) Schmid, R.; Miah, A. M.; Sapunov, V. N. *Phys. Chem. Chem. Phys.* **2000**, *2*, 97−102.
(80) Tawa, G. J.; Topol, I. A.; Burt, S. K.; Caldwell, R. A.; Rashin, A. A. *J. Chem. Phys.* **1998**, *109*, 4852−4863.
(81) Tissandier, M. D.; Cowen, K. A.; Feng, W. Y.; Gundlach, E.; Cohen, M. H.; Earhart, A. D.; Coe, J. V.; Tuttle, T. R. *J. Phys. Chem. A* **1998**, *102*, 7787−7794.
(82) Fawcett, W. R. *J. Phys. Chem. B* **1999**, *103*, 11181−11185.
(83) Zhan, C.-G.; Dixon, D. A. *J. Phys. Chem. A* **2001**, *105*, 11534−11540.
(84) Palascak, M. W.; Shields, G. C. *J. Phys. Chem. A* **2004**, *108*, 3692−3694.
(85) Grossfield, A.; Ren, P.; Ponder, J. W. *J. Am. Chem. Soc.* **2003**, *125*, 15671−15682.
(86) Marcus, Y. *Chem. Rev.* **1988**, *88*, 1475−1498.
(87) Persson, I.; Jalilehvand, F.; Sandström, M. *Inorg. Chem.* **2002**, *41*, 192−197.
(88) Shannon, R. *Acta Crystallogr., Sect. A: Cryst. Phys., Diffr., Theor. Gen. Crystallogr.* **1976**, *32*, 751−767.
(89) Vchirawongkwin, V.; Hofer, T. S.; Randolf, B. R.; Rode, B. M. *J. Comput. Chem.* **2007**, *28*, 1006−1016.
(90) Burda, J. V.; Pavelka, M.; Šimánek, M. *J. Mol. Struct. (THEOCHEM)* **2004**, *683*, 183−193.
(91) Detellier, C.; Laszlo, P. *J. Am. Chem. Soc.* **1980**, *102*, 1135−1141.
(92) Pauling, L. *The nature of the chemical bond and the structure of molecules and crystals: An introduction to modern structural chemistry*; Cornell University Press: Ithaca, NY, USA, 1960; Vol. *18*.
(93) Jorgensen, W. L.; Gao, J. *J. Phys. Chem.* **1986**, *90*, 2174−2182.
(94) Brugé, F.; Bernasconi, M.; Parrinello, M. *J. Am. Chem. Soc.* **1999**, *121*, 10883−10888.
(95) Meraj, G.; Chaudhari, A. *J. Mol. Liq.* **2014**, *190*, 1−5.
(96) Sobolewski, A. L.; Domcke, W. *J. Phys. Chem. A* **2002**, *106*, 4158−4167.
(97) Blauth, C. M.; Pribil, A. B.; Randolf, B. R.; Rode, B. M.; Hofer, T. S. *Chem. Phys. Lett.* **2010**, *500*, 251−255.
(98) Blumberger, J.; Bernasconi, L.; Tavernelli, I.; Vuilleumier, R.; Sprik, M. *J. Am. Chem. Soc.* **2004**, *126*, 3928−3938.
(99) Ohtaki, H.; Radnai, T. *Chem. Rev.* **1993**, *93*, 1157−1204.
(100) Ramaniah, L. M.; Bernasconi, M.; Parrinello, M. *J. Chem. Phys.* **1999**, *111*, 1587−1591.
(101) Soper, A. *J. Chem. Phys.* **1994**, *101*, 6888−6901.
(102) Rajamani, S.; Ghosh, T.; Garde, S. *J. Chem. Phys.* **2004**, *120*, 4457−4466.
(103) Mukhopadhyay, A.; Fenley, A. T.; Tolokh, I. S.; Onufriev, A. V. *J. Phys. Chem. B* **2012**, *116*, 9776−9783.
(104) Mukhopadhyay, A.; Aguilar, B. H.; Tolokh, I. S.; Onufriev, A. V. *J. Chem. Theory Comput.* **2014**, *10*, 1788−1794.
(105) Thompson, W. H.; Hynes, J. T. *J. Am. Chem. Soc.* **2000**, *122*, 6278−6286.
(106) Lee, H. M.; Kim, D.; Kim, K. S. *J. Chem. Phys.* **2002**, *116*, 5509−5520.
(107) Moučka, F.; Nezbeda, I.; Smith, W. R. *J. Chem. Phys.* **2013**, *139*, No. 124505.
(108) Fyta, M.; Netz, R. R. *J. Chem. Phys.* **2012**, *136*, 124103−124111.
(109) Eisenberg, D. S.; Kauzmann, W. *The Structure and Properties of Water*; Oxford University Press: Oxford, U.K., 1969.
(110) Sangster, M.; Atwood, R. *J. Phys. C: Solid State Phys.* **1978**, *11*, 1541.
(111) Robinson, R. A.; Stokes, R. H. *Electrolyte solutions*; Courier Dover: North Chelmsford, MA, USA, 2002.

DOI: 10.1021/ct500918t
J. Chem. Theory Comput. 2015, 11, 1645−1657